applied sciences

MDPI

Article

Investigation of the Role of the Environment on the Photoluminescence and the Exciton Relaxation of $CsPbBr_3$ Nanocrystals Thin Films

Marco Anni [1,*], Arianna Cretì [2], Yuhai Zhang [3,†], Maria Luisa De Giorgi [1] and Mauro Lomascolo [2]

1 Dipartimento di Matematica e Fisica "Ennio De Giorgi", Università del Salento, Via per Arnesano, 73100 Lecce, Italy; marialuisa.degiorgi@unisalento.it
2 IMM-CNR Institute for Microelectronic and Microsystems, Via per Monteroni, 73100 Lecce, Italy; arianna.creti@cnr.it (A.C.); mauro.lomascolo@cnr.it (M.L.)
3 KAUST Solar Center, Division of Physical Sciences and Engineering, King Abdullah University of Science and Technology, Thuwal 23955-6900, Saudi Arabia; ifc_zhangyh@ujn.edu.cn
* Correspondence: marco.anni@unisalento.it
† Current address: Institute for Advanced Interdisciplinary Research (IAIR), University of Jinan, Jinan 250022, China.

Received: 28 February 2020; Accepted: 18 March 2020 ; Published: 21 March 2020

Abstract: In this work, we present a detailed optical investigation of the effects of the environment on the photoluminescence (PL) spectra and the relaxation dynamics of pristine and aged $CsPbBr_3$ nanocrystal (NC) thin films. We demonstrate that, contrary to previous results on similar NCs, the PL intensity of pristine NCs is higher when the sample is in wet air than in vacuum, due to the passivation of defects reducing the free exciton trapping and the bound excitons non-radiative relaxation. The aged NCs show a PL intensity increase in wet air nine times stronger than the pristine ones, due to an interplay between static and dynamic effects, increasing the number of emitting NCs and reducing the non-radiative recombination rate of free excitons. These results improve the understanding of the possible interactions between perovskite NCs and the environment, which could be relevant for the development of optical gas sensors exploiting perovskite NCs.

Keywords: lead halide perovskites; nanocrystals; photoluminescence; time resolved photoluminescence; gas sensors

1. Introduction

Lead halide perovskites are receiving much attention as potentially interesting novel active materials for electronic, optoelectronic, and photonic devices, due to their unique combination of the active properties typical of semiconductors, wide degrees of freedom for their engineering, and possible realization and deposition with easy techniques.

In particular, perovskite nanocrystals (NCs) are very interesting due to the possibility to engineer the optical properties by acting on the chemical composition [1], the size, the shape [2,3], and even the crystalline packing dimensionality within each NC [4]. Moreover, efficient NCs electroluminescence [5] and low threshold amplified spontaneous emission [6–9] have been demonstrated, thus proposing them as possible active materials in LEDs and lasers.

Despite the very rapid performance increase of perovskite-based solar cells [10], LEDs [11], and lasers [12], the applicative perspectives of these materials are currently limited by the lack of long term stability, thus strongly stimulating the research on the understanding of the processes leading to their degradation.

To date, it has been demonstrated that lead halide perovskites can be degraded by many factors such as temperature [13], light exposure [13–17], and interaction with oxygen and moisture [18–21]. Interestingly, despite the reports of material degradation due to its interaction with air, several experiments demonstrated that the interaction with oxygen and wet air can also improve the light emission and the device performances of bulk polycrystalline thin films [22–25] and single crystals [26,27]. This effect, typically reversible, is generally ascribed to the oxygen passivation of halide vacancies taking place at the air–perovskite interface, which decreases the excitation non-radiative decay rate, thus increasing the photoluminescence (PL) intensity and decreasing the PL decay rate [22–27].

The evidence that the optical properties variation is mainly related to the interaction between the perovskite surface and the atmosphere allows expecting a strong environment dependence of the emission properties of NCs, characterized by a much higher surface/volume ratio. Despite this, the effects of the environment on the optical properties of lead halide perovskites NCs have been surprisingly poorly investigated to date, with only few experiments on $CsPbBr_3$ nanocubes grown by hot-injection method, curiously finding contradictory results. In particular, the PL intensity in air has been reported to be lower than in vacuum [3,28], or not affected by the environment [27]. These results are different from the ones on single crystals, bulk polycrystalline thin films, and even nanosheets and nanowires [3], all showing a PL intensity enhancement in air.

In this study, we investigated the role of the synthesis method and of the sample aging on the PL spectra and on the exciton relaxation dependence on the environment in thin films of high quality $CsPbBr_3$ NCs grown by a co-precipitation method. We demonstrate that, differently from what is observed in NCs grown by hot-injection, the PL intensity is higher in wet air (WA, relative humidity $\approx$50%) than in vacuum (V) both in fresh (#F) and in aged (#A) films, ascribed to reversible defects passivation. We also show that the interaction with WA results both in static and in dynamic effects, leading to a variation of the number of emitting NCs and of the exciton relaxation pathways. In Sample #F, the main effects are a decrease of free exciton (FE) trapping, increasing the relative weight of FE radiative recombination, and the suppression of a non-radiative decay process for bound excitons (BE). The increase of surface defects in Sample #A [29] results in a PL intensity increase in WA about nine times stronger than that of Sample #F, due the combination of a strong static increase of the number of emitting NCs and of a reduction of the non-radiative decay rate of FE.

Our results improve the understanding of the possible effects on the perovskite NCs luminescence of the interaction with the atmosphere and on their dependence on the NCs preparation method.

2. Results

The shape and size of the NCs were characterized by TEM measurements, evidencing (see Figure 1) a parallelepiped shape, with an average width of 5.0 $\pm$ 1.5 nm and an average length of 21 $\pm$ 7 nm. The as-prepared thin film shows a photoluminescence quantum yield (PLQY) as high as 88%, evidencing the high optical quality of the NCs.

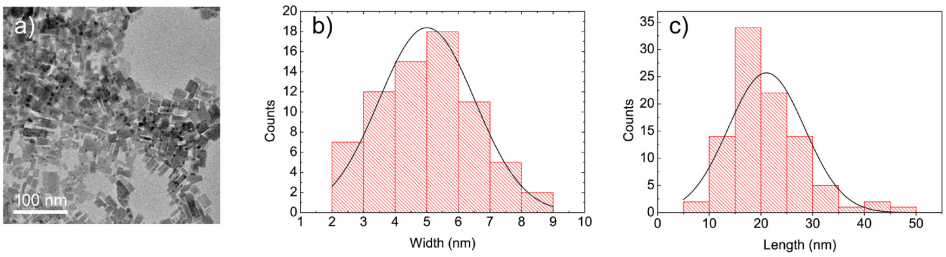

Figure 1. (**a**) TEM image of the $CsPbBr_3$ NCs evidencing a parallelepiped shape; (**b**) distribution of the NCs width (columns) and best fit Gaussian curve; and (**c**) distribution of the NCs length (columns) and best fit Gaussian curve.

The typical PL spectrum of Sample #F in V (see Figure 2a) shows an asymmetric line shape, with a PL peak at about 2.40 eV (517 nm) and a full width at half maximum (FWHM) of 128 meV (28 nm). The line shape can be well reproduced by a best fit with two Gaussian bands peaked at 2.3873 and 2.405 eV and with a FWHM of 149 and 50 meV, respectively. Similar spectra have been reported in the literature for $CsPbBr_3$ NCs films, ascribing the broad band at low energy to excitons bound to defects (BE) and the narrow band at higher energy to free excitons (FE) [30,31].

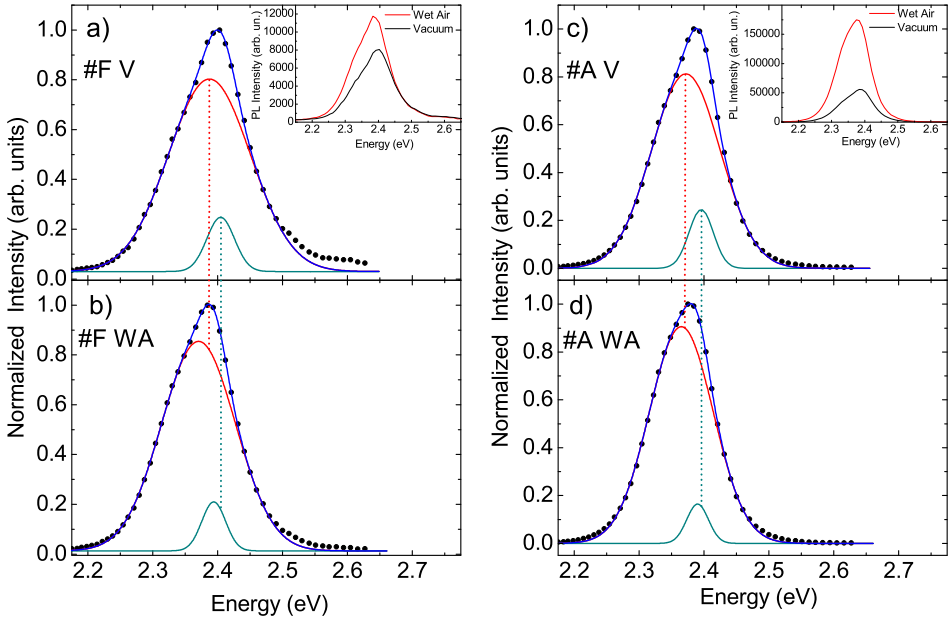

Figure 2. PL spectrum of Samples #F and #A in Vacuum (V) and Wet-Air (WA) atmosphere: (**a**) Sample #F in V; (**b**) Sample #F in WA; (**c**) Sample #A in V; and (**d**) Sample #A in WA. The black dots are the experimental data, and the red, dark cyan, and blue lines are the best fit curves of the BE, FE, and total emission, respectively. All spectra are normalized to 1 for clarity. The insets show the non-normalized PL spectra in V and WA of Sample #F (inset of frame (**a**)) and Sample #A (inset of frame (**c**)), evidencing the clear intensity increase in WA.

The PL intensity presents a quite stable value during continuous laser irradiation (see Figure 3a) with signal variation within 3% around the average values. When the sample atmosphere is changed from V to WA, we observe (see inset of Figures 2a and 3a) an intensity increase by a factor 1.3 (about 30%), and the signal attests itself to the new value within the WA recovering time (less than 5 s). To evaluate the generality of this result the same experiment has been performed also on different positions on the sample, always finding a relative PL intensity increase of about 30%.

Despite the apparently unchanged PL spectrum line shape (see Figure 2b), we observe that the atmosphere variation also affects the BE and FE band peak energy and their FWHM. In particular (see Figure 2b and Table 1), both bands show a small, but evident, red-shift in WA of 16.8 and 11.1 meV for the BE and FE emission band, respectively, and become narrower. These effects are fully reversible and the PL spectrum intensity, the band peak energy, and the FWHM come back to the initial values when the sample chamber is evacuated, thus changing back the atmosphere from WA to V.

Table 1. Best fit values of the peak energy (E), the FWHM, and the integrated intensity (A) of the two best fit Gaussians. The amplitude values are normalized to the integrated PL intensity in V, in order to better evidence their relative variation in WA.

Sample	E_1 (eV)	$FWHM_1$ (meV)	A_1	E_2 (eV)	$FWHM_2$ (meV)	A_2
#F V	2.3873 ± 0.0009	149 ± 2	0.913 ± 0.018	2.405 ± 0.002	50 ± 6	0.087 ± 0.017
#F WA	2.3705 ± 0.0005	134.4 ± 0.9	1.209 ± 0.010	2.3939 ± 0.0009	43 ± 3	0.91 ± 0.09
#A V	2.3720 ± 0.0003	125.1 ± 0.5	0.903 ± 0.005	2.3955 ± 0.0004	44.5 ± 1.3	0.097 ± 0.004
#A WA	2.3650 ± 0.0004	116.1 ± 0.6	2.64 ± 0.02	2.3901 ± 0.0008	40 ± 3	0.163 ± 0.016

To probe the role of the NCs surface quality on the interaction with the environment, the same experiment was also performed on a sample aged by exposure to WA in dark for one month (Sample #A). The long exposure of $CsPbBr_3$ to WA results in an irreversible degradation, mainly due to surface decomposition and generation of surface trap states [29]. Sample #A in V shows (see Figure 2c) a line shape similar to the one of Sample #F, again resulting from the superposition of a broad band at low energy and a narrower band at higher energy ascribed to BE and FE, respectively. Both bands are slightly red-shifted (see Table 1) by about 15 meV for the BE and 10 meV for the FE with respect to the corresponding bands of Sample #F, and are narrower.

When the sample atmosphere is switched to WA, we observe (see inset of Figures 2c and 3b) a PL intensity increase qualitatively similar to the one of Sample #F, but with a significantly different quantitative intensity variation. In particular, the intensity emission in WA is 2.8 times higher than the one in V, thus about nine times higher than the one of Sample #F. The peak position of the BE and FE emission bands is red-shifted in WA by about 7.0 and 5.4 meV, respectively, and a FWHM reduction is observed. In addition, also in this sample, the observed variations are fully reversible if the vacuum is restored in the sample chamber.

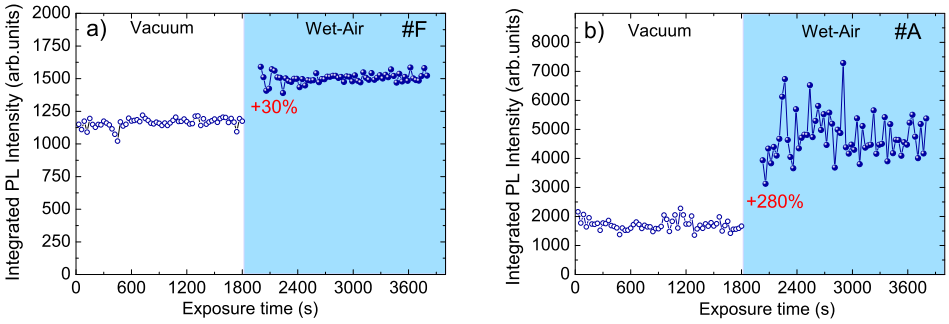

Figure 3. Integrated intensity during time under continuous laser irradiation in vacuum and wet air evidencing the clear intensity increase in wet air with respect to the value in vacuum: Sample #F (**a**); and Sample #A (**b**).

To get a deeper insight in the origin of the PL intensity dependence on the different environmental conditions, we performed time resolved spectroscopy by recording TR-PL in experimental conditions similar to those used for CW-PL in Figure 3.

The TR-PL signal of Sample #F in vacuum shows (see Figure 4a) a non-exponential relaxation, which can be reproduced by the superposition of three exponential decays:

$$I(t) = y_0 + A_1 e^{-t/\tau_1} + A_2 e^{-t/\tau_2} + A_3 e^{-t/\tau_3} \quad (1)$$

The multi-exponential decay analysis evidences (see Figure 3a) two fast recombination processes with time constants $\tau_1 \approx 1.9$ ns and $\tau_2 \approx 11.5$ ns, and a slower process with time constant $\tau_3 \approx 70$ ns.

To ascribe these decay processes, we initially observe that the TR-PL have been recorded at the PL spectrum maximum; thus, considering that the FE band lies within the spectral broadening of BE one, the TR-PL signals contains the superposition of the BE and FE relaxation dynamics.

Moreover, the presence of different decay times between a few and hundreds of nanoseconds has already been observed in $CsPbBr_3$ NCs [32], and allows tentatively ascribing τ_1 to FE trapping, τ_2 to FE recombination, and τ_3 to BE relaxation. The relative amplitudes of these processes are 68.4%, 27.4%, and 4.2%, respectively.

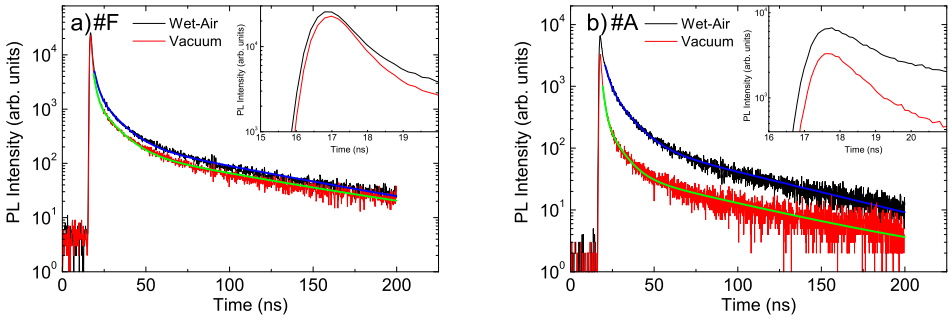

Figure 4. TR-PL traces in V (red line) and WA (black line) of: Sample #F (**a**); and Sample #A (**b**). The green and blue lines are the corresponding best fit curves with a three exponential decay. Insets: Magnification of the peak signal, evidencing that the peak value is basically not affected by the V to WA transition in Sample #F while it clearly increases in Sample #A.

When the atmosphere changes from V to WA, the following effects are observed for Sample #F (see Figures 4a and 5a):

1. The peak intensity slightly increases (about 13%) (see inset of Figure 4a).
2. The two faster decay times remain essentially unchanged ($\tau_1 \approx 1.9$ ns and $\tau_2 \approx 11.5$ ns), while a clear increase of the longest decay time τ_3 from about 70 ns to about 100 ns is observed.
3. The pre-exponential amplitude of the fastest process A_1 slightly decreases (about 4%), while the amplitudes A_2 and A_3 increase of about 40% and 36%, respectively.

Sample #A in vacuum shows a decay dynamic qualitatively similar to the one of Sample #F, but with decreased lifetimes down to $\tau_1 \approx 1.2$ ns, $\tau_2 \approx 7.5$ ns, and $\tau_3 \approx 65$ ns, and a clearly stronger relative contribution of the FE trapping (relative amplitude 85.7%) and a reduced relative amplitude of FE relaxation (12.9%) and BE relaxation (1.4%).

The relaxation dynamics variation of Sample #A when the atmosphere is changed from V to WA is very different from the one of Sample #F (see Figures 4b and 5b), in particular:

1. The peak intensity increases of about 2 times (see inset of Figure 4b).
2. A clear increase of the two faster decay times is observed (τ_1 from 1.2 to about 2.0 ns and τ_2 from about 7.5 to about 9.8 ns), while the slowest time τ_3 remains basically constant at about 65 ns.
3. All the pre-exponential amplitudes clearly increase of about 1.9, 4.3, and 3.9 times for A_1, A_2, and A_3, respectively.

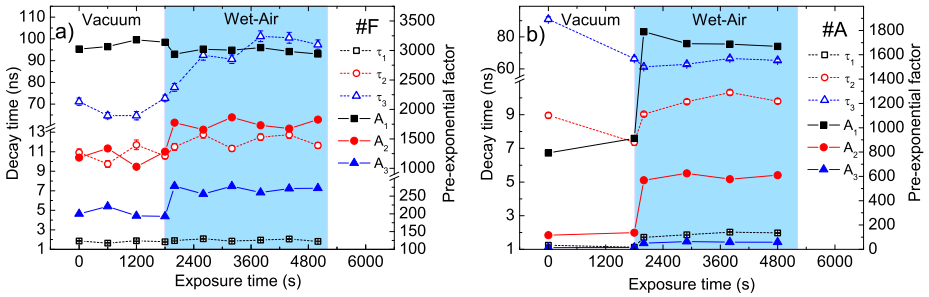

Figure 5. Pre-exponential amplitudes and corresponding decay times during irradiation in V and WA for: Sample #F (**a**); and Sample #A (**b**).

3. Discussion

To understand the processes leading to the PL intensity dependence on the environment in Sample #F and the origin of the strongly different behavior observed in Sample #A, it is first useful to remind that the PL intensity increase observed in both samples is qualitatively similar to the one reported both for lead halide perovskites polycrystalline thin films [22–25] and single crystals [26,27]. In all these systems, the PL intensity increase in WA has been ascribed to oxygen or moisture induced passivation of halide vacancies, which reduces the non-radiative decay rate, thus increasing the PLQY and the PL lifetime. In particular, in fully inorganic perovskites, the separate investigation of the role of the oxygen and of the moisture content allowed to conclude that the moisture effect is much weaker than the oxygen one [27]. On the contrary the few previous experiments on $CsPbBr_3$ NCs films evidenced a very different behavior, with the lack of any PL intensity variation due to the interaction with WA [27], or even an opposite PL intensity variation in WA (quenching instead of enhancement) [3,28], ascribed to the lack of halide (Br^-) vacancies on the NCs surface in the first experiment and to a different kind of defects on the NCs surface with respect to bulk polycrystalline films or single crystals in the second.

The presence of PL enhancement in WA in our samples thus suggests that the co-precipitation growth method leads to the formation of NCs with a higher density of bromine vacancies on the surface with respect to NCs grown by hot-injection. It is also important to underline that the very high PLQY of the just deposited films and the relatively small PL intensity increase of Sample #F suggest a defect density much smaller than the one of bulk polycrystalline films and single crystals, typically showing much lower initial PLQY and much higher PL enhancement in WA [22–27]. We also underline that the observed small red-shift and the narrowing of the FE and BE bands are consistent with previous results on $MAPbI_3$ thin films [24], ascribed to defects passivation without irreversible degradation. Further experiments, beyond the scope of the current paper, will be necessary to determine if this passivation is mainly due to oxygen or moisture. The analysis of the PL relaxation dynamics variation in WA allows gaining a deeper insight into the effects of the interaction with WA on the exciton relaxation pathways. In particular, the slight increase of the TR-PL peak value evidences the presence of a corresponding increase of the number of emitting sites (static interaction) [3], qualitatively consistent with the increase of the number of emitting grains observed in polycrystalline $MAPbI_3$ films in WA [22]. Moreover, beyond the static effects, the interaction with WA also modifies the PL relaxation dynamics, which become slower in WA. While this effect can be described as an average lifetime increase, also observed in $MAPbI_3$ films [23], our data evidence that this effect, in our sample, cannot be simply explained by the suppression of a non-radiative decay channel that increases the lifetimes. In particular, we observe that no variations are present both in the FE trapping lifetime τ_1 and in the FE relaxation time τ_2, while the variation affects the pre-exponential amplitudes, with a reduction of the FE trapping and the increase of the FE relaxation one. This result can be qualitatively ascribed to the complete passivation of defects in a part of the NCs, which then only shows FE recombination, indirectly confirming the low initial defects density. The interaction with WA also affects the BE contribution to the emission, with a clear increase of both the amplitude and of the decay times, evidencing the interplay between static increase of the number of emitting sites and dynamic suppression of a non-radiative decay process of BE.

The role of the defects density on the PL intensity increase in WA can be investigated by looking at the results on Sample #A, which is expected to have a lower surface quality due to the prolonged interaction with WA leading to the aging [29]. This sample actually shows a PL intensity increase in WA of 2.8 times, thus about nine times higher than that of Sample #F. This result is consistent with an increased defects density.

The presence of a higher defects density in Sample #A is also confirmed by the increase of the relative amplitude of exciton trapping that, in V, is about 86% with respect to 68% of Sample #F. The analysis of the variations of the TR-PL signals in WA allows observing that most of this PL increase (about 70%) is of static nature, as evidenced by the increase of two times of the TR-PL peak

signal. The static effects modifies all the pre-exponential amplitudes but with differences in the relative increase. In particular, the exciton trapping amplitude shows an increase (about two times) lower than the FE and BE recombination increases (both about four times), resulting in relative decrease of the FE trapping and a correspondent increase of the FE recombination contribution to the PL relaxation in WA.

In Sample #A, we observe that this reduction of the relative importance of FE trapping takes place together with a clear increase of both the trapping lifetime τ_1 and the FE recombination lifetime τ_2, evidencing both a reduction of the FE trapping probability and of the FE non-radiative relaxation. Interestingly, no variations of the BE lifetime τ_3 are now present, evidencing that the states generating the BE emission are no longer able to interact with the atmosphere, likely due to irreversible oxidation of Sample #A.

4. Materials and Methods

4.1. Synthesis of NCs

Chemicals: Lead (II) bromide (PbBr2, 99.0 %) and caesium acetate (CsAc, 99.99% trace metals basis) were purchased from Aladdin. Octylamine (OcAm, 99%) and octanoic acid (OcAc, 99%) were purchased from Macklin. 1-propanol (PrOH), n-Hexane (Hex, 99.5%), and toluene (TOL, 99.5%) were purchased from Tianjin Fuyu Fine Chemical Co., Ltd, China. All chemicals were used without any further purification. $CsPbBr_3$ was synthesized by a co-precipitation method. Typically, 384 mg CsAc, 12 mL 1-PrOH, and 24 mL Hex were loaded into a 100 mL vial and stirred at ambient condition to form a transparent solution A. Then, 3.67 g $PbBr_2$ were added into a 20 mL vial, followed by 5.4 mL 1-PrOH, 5.4 mL OcAc, and 5.4 mL OcAm. The mixture was heated at 90 °C in air under vigorous stirring to form solution B. After complete dissolution of the $PbBr_2$ salt, the hot solution B was quickly injected into the prepared solution A under vigorous stirring. The color of the mixture turned yellow immediately, indicating the formation of NCs. Finally, the mixture was centrifuged at 4000 rpm, and the wet pellet of the NCs was dispersed in 36 mL toluene for further characterization. The colloid gradually turned from yellow to green in a few days, and stayed unchanged for at least eight months.

4.2. Samples Preparation and Characterization

The NCs shape and size distribution was investigated by TEM measurements with a JEOL 2100F transmission electron microscope under 200-kV voltage.

The PLQY of thin-film sample was then measured in an integrated sphere coupled in an Edinburgh FS5 spectrometer under 365-nm excitation.

The fresh film Sample #F was deposited by drop casting from a 1.5% in weight solution in toluene on a quartz slide and let dry naturally. The aged Sample #A was obtained by keeping Sample #F in dark and wet air (relative humidity about 50%) for one month.

4.3. PL and Time Resolved PL Measurements

PL and TR-PL measurements were performed by exciting the samples with a solid state pulsed laser (mod. PLP-10, Hamamatsu), providing pulse of about 58 ps, at a wavelength of 400 nm, and at a repetition rate of 1 MHz. The maximum peak power was about 70 mW. The PL was dispersed by an iHR320 (focal length of 0.32 m) Horiba monochromator equipped with a Peltier cooled Hamamatsu photomultiplier (Head-on mod R943-02), operating in single photon counting. Time-correlated single photon counting (TCSPC) technique was used to record TR-PL in the spectral visible range by using an Edinburg Instruments TCC900 TSCPC electronics card. The temporal resolution of the system is about 0.46 ns. In the study of the PL signal stability, the emission signal was also collected in backscattering configuration by an optical fiber (diameter 1mm) and dispersed by a Triax320 (focal length of 0.32 m) Jobin–Yvon monochromator, coupled to a Peltier cooled CCD in kinetic acquisition mode. PL and TR-PL experiments were carried out in vacuum (V) and wet air (WA) atmosphere,

by putting the samples in a chamber connected to a vacuum-pump. The V pressure level (10^{-3} mbar) and the recovering of WA condition occurred in less than 5 s, after switching the chamber environment from V to WA or vice versa. The environmental relative humidity was about 50%.

5. Conclusions

We investigated the effects of the interaction with WA on the luminescence properties of thin films of high quality NCs grown by a co-precipitation method, evidencing a strongly different behavior with respect to the NCs grown by hot-injection. We demonstrated that the PL intensity increase in WA with respect to V is due to the interplay between static and dynamic effects, with quantitative importance and specific effects on the exciton relaxation processes strongly modified by the sample aging. These results, beyond improving the understanding of the possible interaction with the environment of perovskite NCs, are also relevant for the development of optical gas sensors based on these materials. Further experiments, beyond the scope of the current paper, could help in obtaining a deeper understanding of the details of the interaction between NCs realized by co-precipitation and the environment. For example, a systematic investigation of the effects of the moisture and oxygen relative content could allow confirming that the main defect passivation is due to oxygen and determining the relative importance of the surface related emission on the whole film emission. Conversely, the exposure to other kinds of oxygen rich or oxygen poor vapors could allow better understanding the correlation between the emission properties variation and the chemical nature of the vapors.

Author Contributions: Conceptualization, M.A., A.C., Y.Z., M.L.D.G., and M.L.; Data curation, M.A., A.C., and M.L.; Investigation, A.C., Y.Z., and M.L.; Supervision, M.A. and M.L.; Writing—original draft, M.A.; and Writing—review and editing, M.A., A.C., Y.Z., M.L.D.G., and M.L. All authors have read and agreed to the published version of the manuscript.

Funding: This research received no external funding.

Acknowledgments: Omar F. Mohammed from KAUST Solar Center (Kingdom of Saudi Arabia) is acknowledged for the possibility to exploit his know-how on the nanocrystals synthesis, necessary for the realization of the samples used in this experiment.

Conflicts of Interest: The authors declare no conflict of interest.

References

1. Protesescu, L.; Yakunin, S.; Bodnarchuk, M.I.; Krieg, F.; Caputo, R.; Hendon, C.H.; Yang, R.X.; Walsh, A.; Kovalenko, M.V. Nanocrystals of Cesium Lead Halide Perovskites (CsPbX3, X = Cl, Br, and I): Novel Optoelectronic Materials Showing Bright Emission with Wide Color Gamut. *Nano Lett.* **2015**, *15*, 3692–3696. [CrossRef] [PubMed]
2. Wang, S.; Yu, J.; Zhang, M.; Chen, D.; Li, C.; Chen, R.; Jia, G.; Rogach, A.L.; Yang, X. Stable, Strongly Emitting Cesium Lead Bromide Perovskite Nanorods with High Optical Gain Enabled by an Intermediate Monomer Reservoir Synthetic Strategy. *Nano Lett.* **2019**, *19*, 6315–6322. [CrossRef] [PubMed]
3. Rodá , C.; Abdelhady, A.L.; Shamsi, J.; Lorenzon, M.; Pinchetti, V.; Gandini, M.; Meinardi, F.; Manna, L.; Brovelli, S. O_2 as a molecular probe for nonradiative surface defects in CsPbBr3 perovskite nanostructures and single crystals. *Nanoscale* **2019**, *11*, 7613–7623. [CrossRef] [PubMed]
4. Yang, H.; Zhang, Y.; Pan, J.; Yin, J.; Bakr, O.M.; Mohammed, O.F. Room-Temperature Engineering of All-Inorganic Perovskite Nanocrsytals with Different Dimensionalities. *Chem. Mat.* **2017**, *29*, 8978–8982. [CrossRef]
5. Park, J.H.; Lee, A.y.; Yu, J.C.; Nam, Y.S.; Choi, Y.; Park, J.; Song, M.H. Surface Ligand Engineering for Efficient Perovskite Nanocrystal-Based Light-Emitting Diodes. *ACS Appl. Mater. Interfaces* **2019**, *11*, 8428–8435. [CrossRef]
6. Yakunin, S.; Protesescu, L.; Krieg, F.; Bodnarchuk, M.I.; Nedelcu, G.; Humer, M.; De Luca, G.; Fiebig, M.; Heiss, W.; Kovalenko, M.V. Low-Threshold Amplified Spontaneous Emission and Lasing From Colloidal Nanocrystals of Caesium Lead Halide Perovskites. *Nat. Commun.* **2015**, *6*, 8056. [CrossRef]

7. Pan, J.; Sarmah, S.P.; Murali, B.; Dursun, I.; Peng, W.; Parida, M.R.; Liu, J.; Sinatra, L.; Alyami, N.; Zhao, C.; et al. Air-Stable Surface-Passivated Perovskite Quantum Dots for Ultra-Robust, Single- and Two-Photon-Induced Amplified Spontaneous Emission. *J. Phys. Chem. Lett.* **2015**, *6*, 5027–5033. [CrossRef]
8. Balena, A.; Perulli, A.; Fernandez, M.; De Giorgi, M.L.; Nedelcu, G.; Kovalenko, M.V.; Anni, M. Temperature Dependence of the Amplified Spontaneous Emission from CsPbBr3 Nanocrystal Thin Films. *J. Phys. Chem. C* **2018**, *122*, 5813–5819. [CrossRef]
9. De Giorgi, M.L.; Krieg, F.; Kovalenko, M.V.; Anni, M. Amplified Spontaneous Emission Threshold Reduction and Operational Stability Improvement in CsPbBr3 Nanocrystals Films by Hydrophobic Functionalization of the Substrate. *Sci. Rep.* **2019**, *9*, 17964. [CrossRef]
10. National Renewable Energy Laboratory. Research Cell Record Efficiency Chart. Available online: https://www.nrel.gov/pv/assets/images/efficiency-chart.png (accessed on 20 March 2020).
11. Lin, K.; Xing, J.; Quan, L.N.; de Arquer, F.P.G.; Gong, X.; Lu, J.; Xie, L.; Zhao, W.; Zhang, D.; Yan, C.; et al. Perovskite light-emitting diodes with external quantum efficiency exceeding 20 per cent. *Nature* **2018**, *562*, 245–248. [CrossRef]
12. De Giorgi, M.L.; Anni, M. Amplified Spontaneous Emission and Lasing in Lead Halide Perovskites: State of the Art and Perspectives. *Appl. Sci.* **2019**, *9*, 4591. [CrossRef]
13. Juarez-Perez, E.J.; Ono, L.K.; Maeda, M.; Jiang, Y.; Hawash, Z.; Qi, Y. Photodecomposition and thermal decomposition in methylammonium halide lead perovskites and inferred design principles to increase photovoltaic device stability. *J. Mater. Chem. A* **2018**, *6*, 9604–9612. [CrossRef]
14. Quitsch, W.A.; de Quilettes, D.W.; Pfingsten, O.; Schmitz, A.; Ognjanovic, S.; Jariwala, S.; Koch, S.; Winterer, M.; Ginger, D.S.; Bacher, G. The Role of Excitation Energy in Photobrightening and Photodegradation of Halide Perovskite Thin Films. *J. Phys. Chem. Lett.* **2018**, *9*, 2062–2069. [CrossRef] [PubMed]
15. Motti, S.G.; Gandini, M.; Barker, A.J.; Ball, J.M.; Srimath Kandada, A.R.; Petrozza, A. Photoinduced Emissive Trap States in Lead Halide Perovskite Semiconductors. *ACS Energy Lett.* **2016**, *1*, 726–730. [CrossRef]
16. Barker, A.J.; Sadhanala, A.; Deschler, F.; Gandini, M.; Senanayak, S.P.; Pearce, P.M.; Mosconi, E.; Pearson, A.J.; Wu, Y.; Srimath Kandada, A.R.; et al. Defect-Assisted Photoinduced Halide Segregation in Mixed-Halide Perovskite Thin Films. *ACS Energy Lett.* **2017**, *2*, 1416–1424. [CrossRef]
17. Li, Y.; Xu, X.; Wang, C.; Ecker, B.; Yang, J.; Huang, J.; Gao, Y. Light-Induced Degradation of CH3NH3PbI3 Hybrid Perovskite Thin Film. *J. Phys. Chem. C* **2017**, *121*, 3904–3910. [CrossRef]
18. Hodes, G.; Cahen, D. Perovskite cells roll forward. *Nat. Photonics* **2014**, *8*, 87–88. [CrossRef]
19. Christians, J.; Miranda Herrera, P.; Kamat, P. Transformation of the excited state and photovoltaic efficiency of CH3NH3PbI3 perovskite upon controlled exposure to humidified air. *J. Am. Chem. Soc.* **2015**, *137*, 1530–1538. [CrossRef]
20. Yun, J.S.; Kim, J.; Young, T.; Patterson, R.J.; Kim, D.; Seidel, J.; Lim, S.; Green, M.A.; Huang, S.; Ho-Baillie, A. Humidity-Induced Degradation via Grain Boundaries of HC(NH2)2PbI3 Planar Perovskite Solar Cells. *Adv. Funct. Mater.* **2018**, *28*, 1705363. [CrossRef]
21. Wang, Q.; Chen, B.; Liu, Y.; Deng, Y.; Bai, Y.; Dong, Q.; Huang, J. Scaling behavior of moisture-induced grain degradation in polycrystalline hybrid perovskite thin films. *Energy Environ. Sci.* **2017**, *10*, 516–522. [CrossRef]
22. Brenes, R.; Guo, D.; Osherov, A.; Noel, N.K.; Eames, C.; Hutter, E.M.; Pathak, S.K.; Niroui, F.; Friend, R.H.; Islam, M.S.; et al. Metal Halide Perovskite Polycrystalline Films Exhibiting Properties of Single Crystals. *Joule* **2017**, *1*, 155–167. [CrossRef]
23. Godding, J.S.; Ramadan, A.J.; Lin, Y.H.; Schutt, K.; Snaith, H.J.; Wenger, B. Oxidative Passivation of Metal Halide Perovskites. *Joule* **2019**, *3*, 2716–2731. [CrossRef]
24. Péan, E.V.; Castro, C.S.D.; Davies, M.L. Shining a light on the photoluminescence behaviour of methylammonium lead iodide perovskite: Investigating the competing photobrightening and photodarkening processes. *Mater. Lett.* **2019**, *243*, 191–194. [CrossRef]
25. Howard, J.M.; Tennyson, E.M.; Barik, S.; Szostak, R.; Waks, E.; Toney, M.F.; Nogueira, A.F.; Neves, B.R.A.; Leite, M.S. Humidity-Induced Photoluminescence Hysteresis in Variable Cs/Br Ratio Hybrid Perovskites. *J. Phys. Chem. Lett.* **2018**, *9*, 3463–3469. [CrossRef] [PubMed]
26. Zhang, H.; Liu, Y.; Lu, H.; Deng, W.; Yang, K.; Deng, Z.; Zhang, X.; Yuan, S.; Wang, J.; Niu, J.; et al. Reversible air-induced optical and electrical modulation of methylammonium lead bromide (MAPbBr3) single crystals. *Appl. Phys. Lett.* **2017**, *111*, 103904. [CrossRef]

27. Wang, Y.; Ren, Y.; Zhang, S.; Wu, J.; Song, J.; Li, X.; Xu, J.; Sow, C.H.; Zeng, H.; Sun, H. Switching excitonic recombination and carrier trapping in cesium lead halide perovskites by air. *Commun. Phys.* **2018**, *1*, 96. [CrossRef]
28. Lorenzon, M.; Sortino, L.; Akkerman, Q.; Accornero, S.; Pedrini, J.; Prato, M.; Pinchetti, V.; Meinardi, F.; Manna, L.; Brovelli, S. Role of Nonradiative Defects and Environmental Oxygen on Exciton Recombination Processes in CsPbBr3 Perovskite Nanocrystals. *Nano Lett.* **2017**, *17*, 3844–3853. [CrossRef]
29. Huang, S.; Li, Z.; Wang, B.; Zhu, N.; Zhang, C.; Kong, L.; Zhang, Q.; Shan, A.; Li, L. Morphology Evolution and Degradation of CsPbBr3 Nanocrystals under Blue Light-Emitting Diode Illumination. *ACS Appl. Mat. Interfaces* **2017**, *9*, 7249–7258. [CrossRef]
30. Lee, S.M.; Moon, C.J.; Lim, H.; Lee, Y.; Choi, M.Y.; Bang, J. Temperature-Dependent Photoluminescence of Cesium Lead Halide Perovskite Quantum Dots: Splitting of the Photoluminescence Peaks of CsPbBr3 and CsPb(Br/I)3 Quantum Dots at Low Temperature. *J. Phys. Chem. C* **2017**, *121*, 26054–26062. [CrossRef]
31. Dey, A.; Rathod, P.; Kabra, D. Role of Localized States in Photoluminescence Dynamics of High Optical Gain CsPbBr3 Nanocrystals. *Adv. Opt. Mat.* **2018**, *6*, 1800109. [CrossRef]
32. Li, J.; Yuan, X.; Jing, P.; Li, J.; Wei, M.; Hua, J.; Zhao, J.; Tian, L. Temperature-Dependent Photoluminescence of Inorganic Perovskite Nanocrystal Films. *RSC Adv.* **2016**, *6*, 78311–78316. [CrossRef]